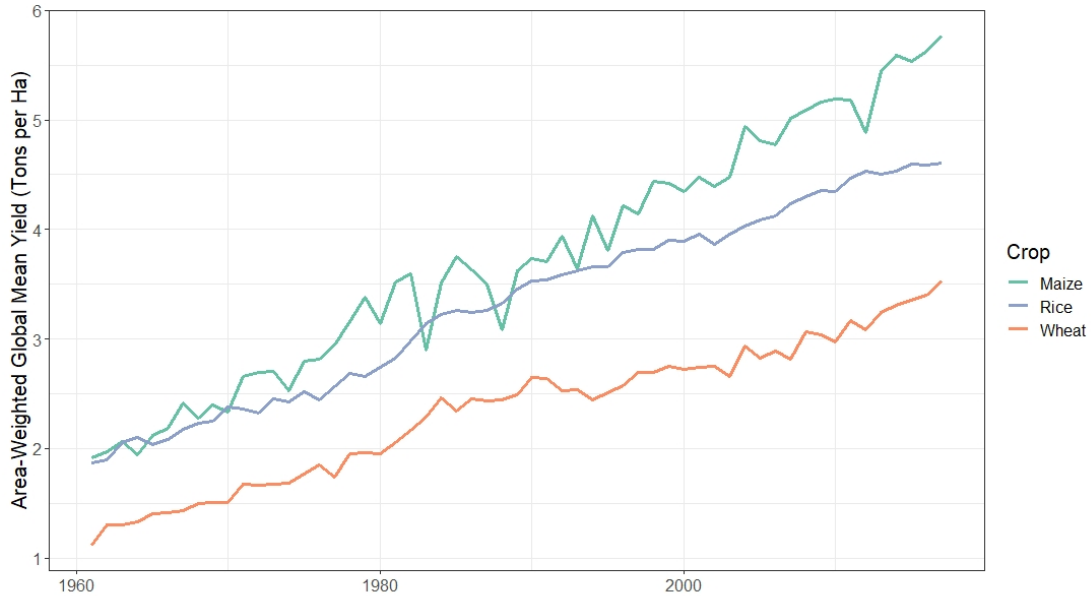
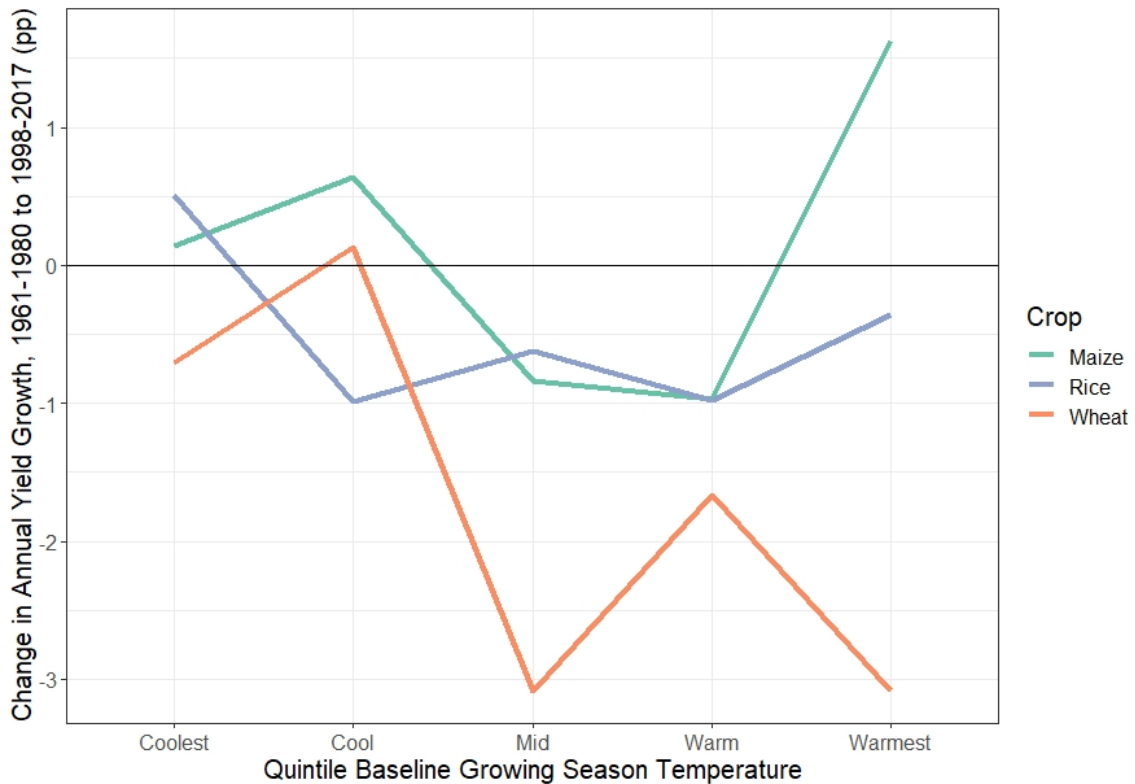


Supplementary Information

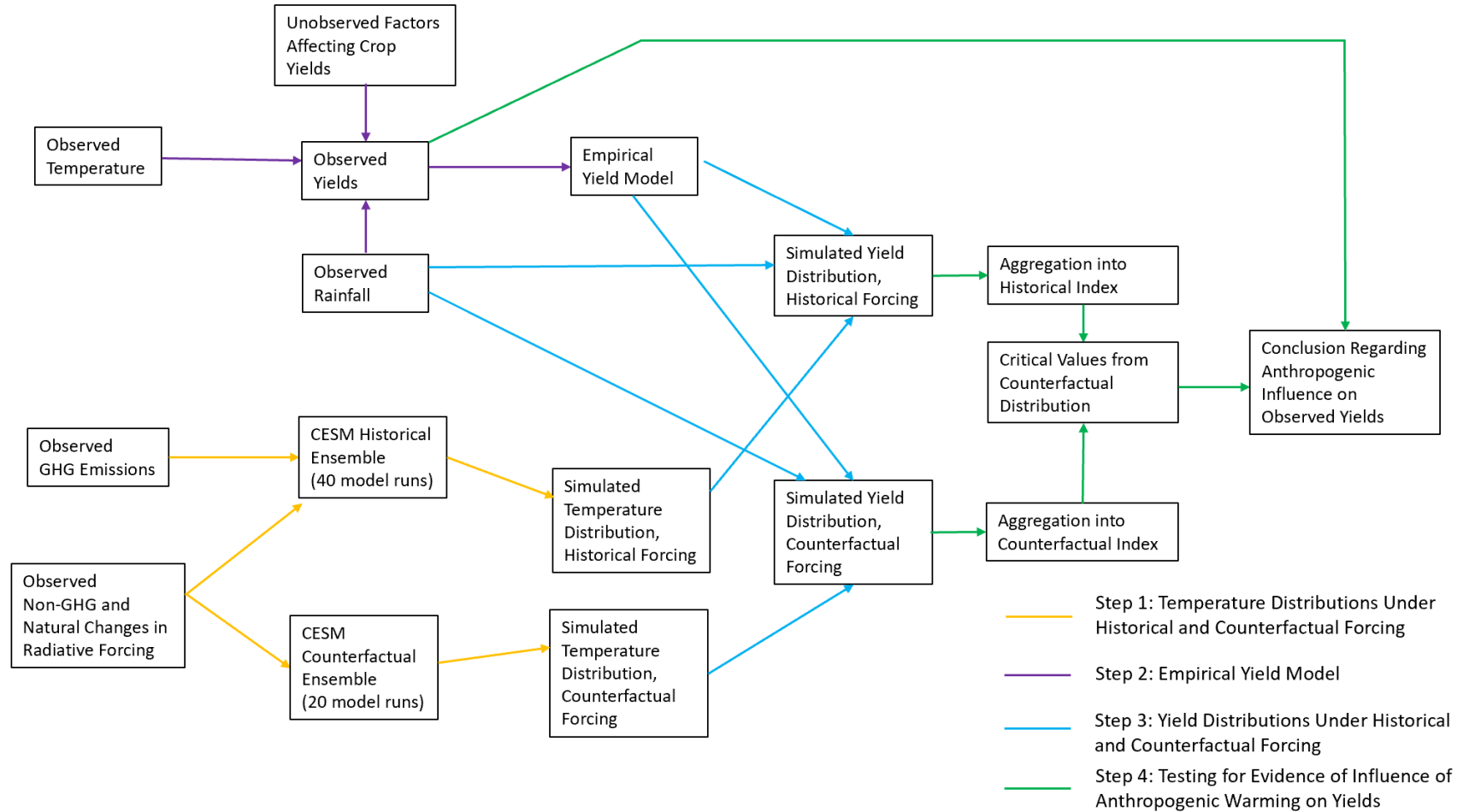
a)



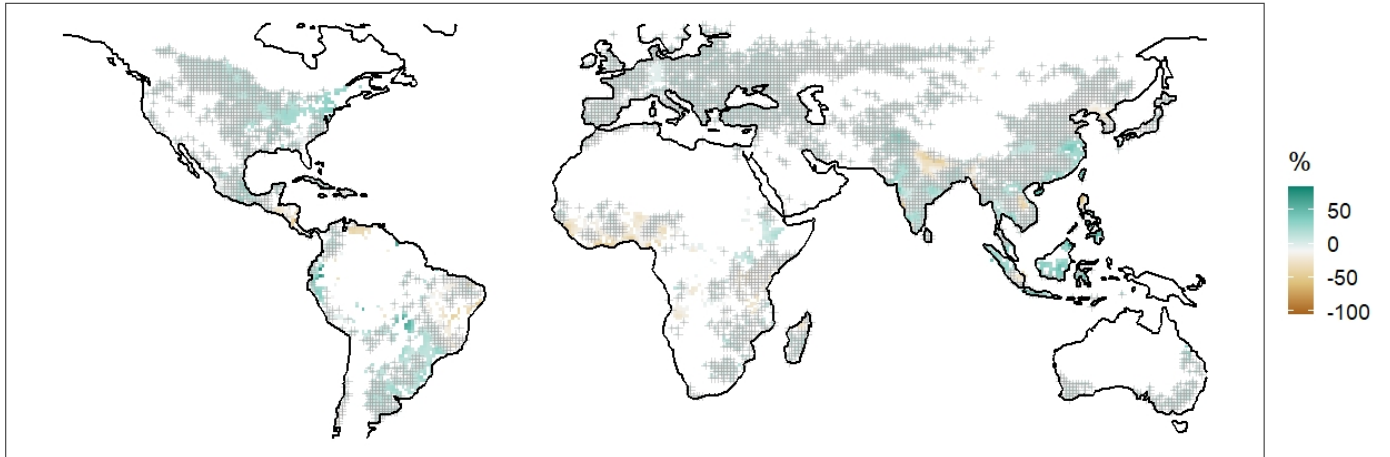
b)



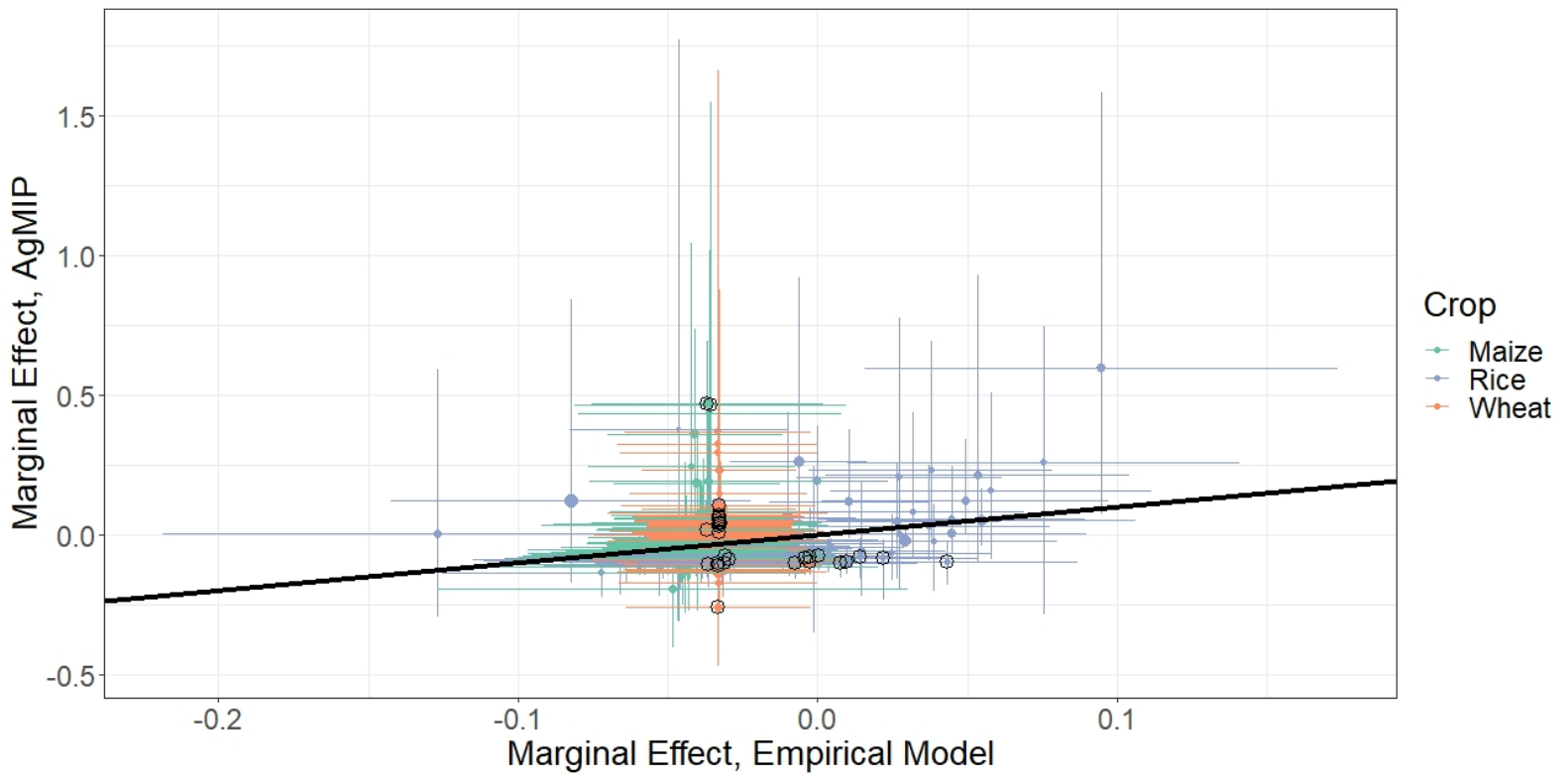
Supplementary Figure 1: a) Global observed, area-weighted yields over the sample period, 1961-2017. b) Observed change in yield growth by crop and distribution of baseline (pre-1981) growing-season temperatures between the first 20 years in the sample (1961-1980) and the last 20 years (1998-2017) in percentage points (pp).



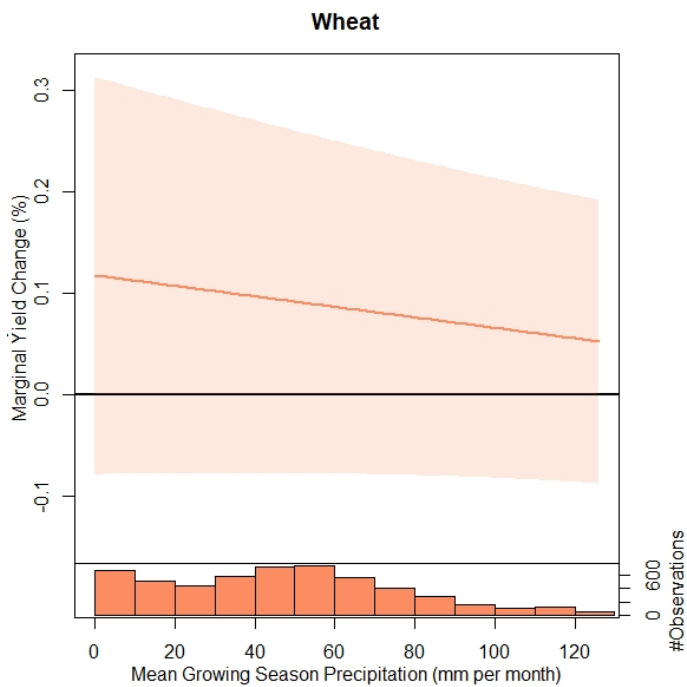
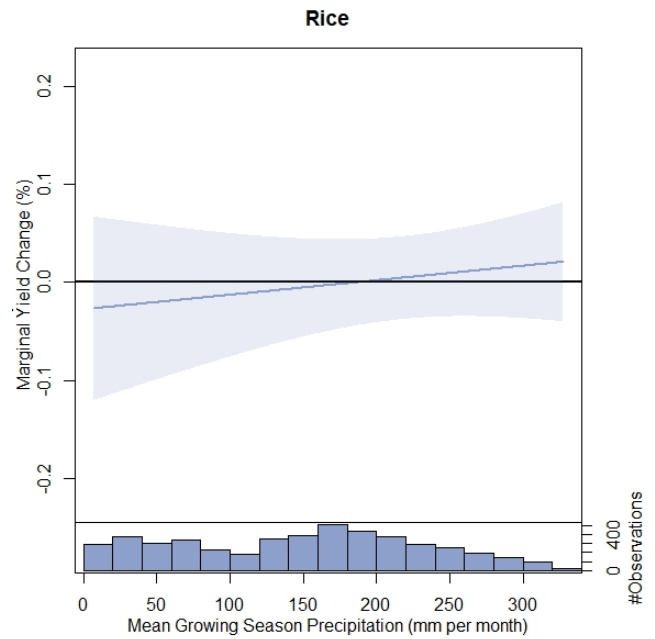
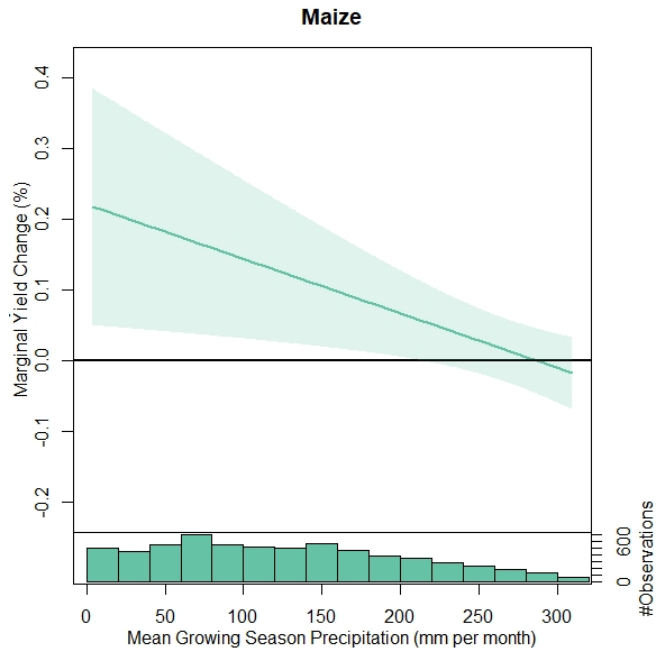
Supplementary Figure 2: Schematic diagram of methodological approach in this paper



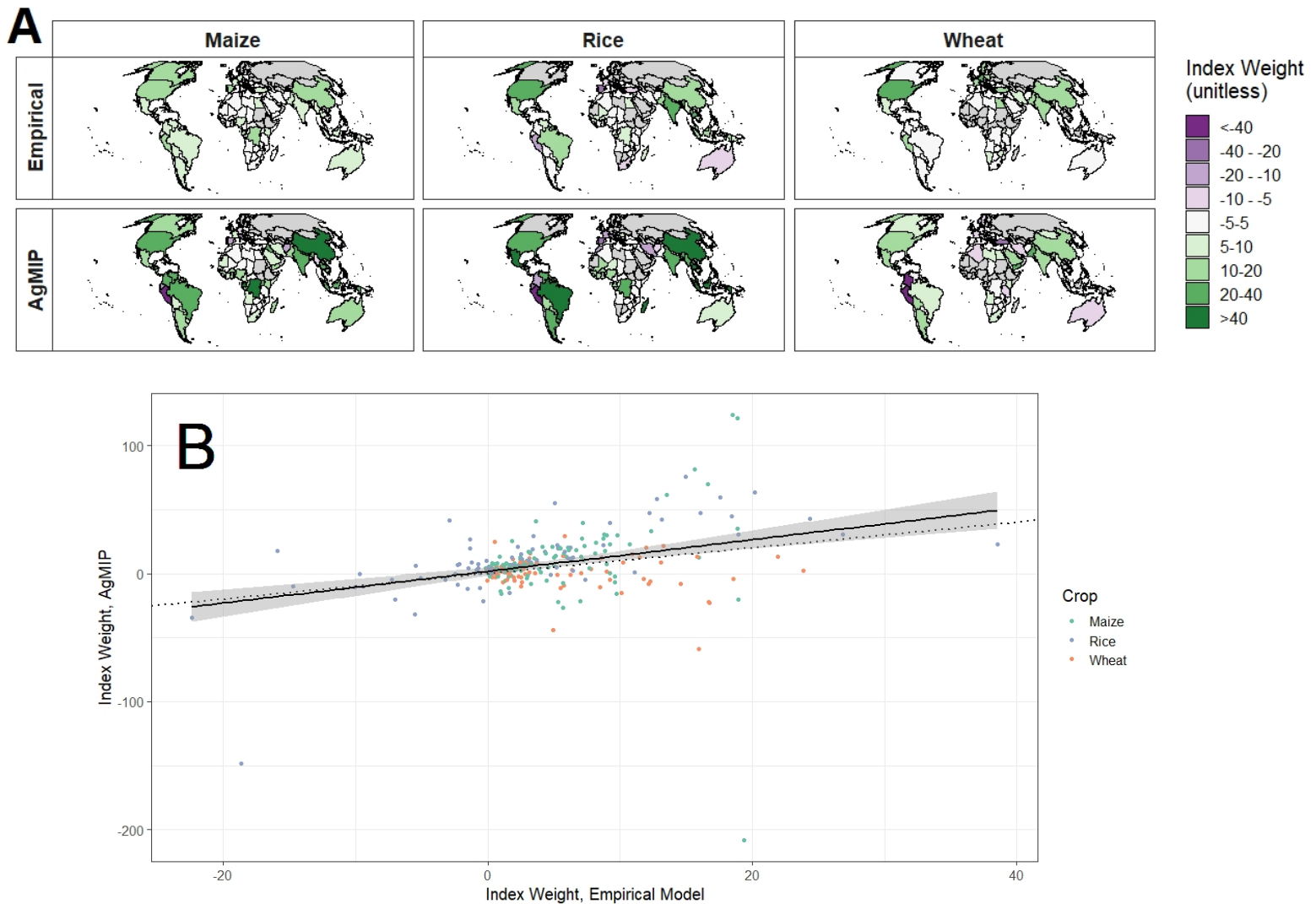
Supplementary Figure 3: Observed change in growing season rainfall over wheat, rice and maize growing areas (grid cells with >50 Ha combined in 2000 (1)) between 1961-1970 and 2008-2017 (2), given as % change relative to baseline period. Growing-season trends for the three crops are a calorie-weighted average of production for each grid cell. Grey crosses indicate areas where the observed change is within the central 95% of the distribution from the counterfactual climate model ensemble that omits greenhouse gas emissions since 1920.



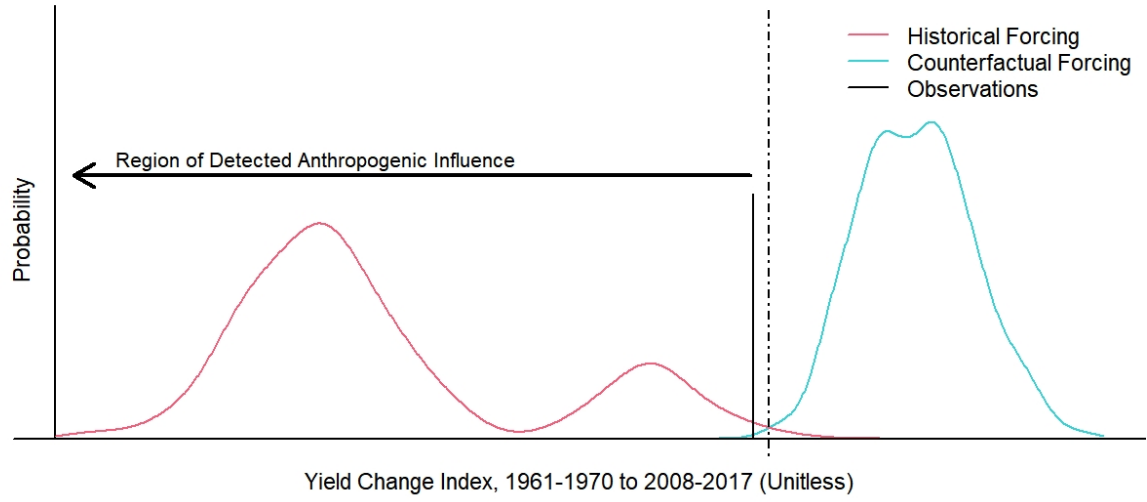
Supplementary Figure 4: Comparison of the distribution of marginal effects of warming across crop-country combinations in the analysis estimated using the empirical crop model (Figure 2) and the mean of the gridded process-based crop models in the AgMIP Phase 2 experiment. Error bars for the empirical model give the 95% confidence interval of the marginal effect. Error bars for AgMIP give the range across the 4 models used in this analysis (Methods). Point size is proportional to log of growing area. The black line gives the 1:1 line and black circles show crop-country combinations where uncertainty ranges from the two estimates are non-overlapping.



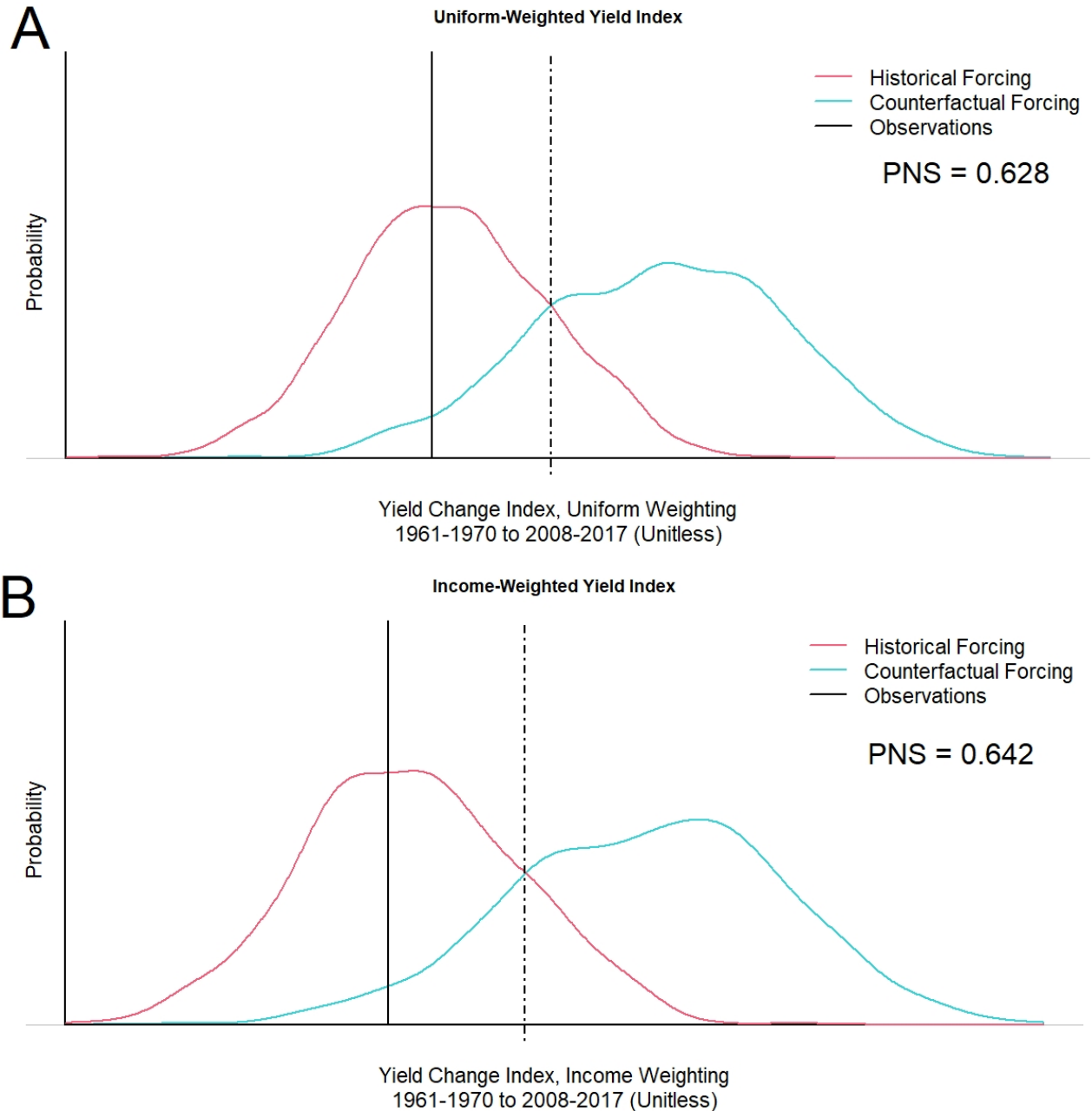
Supplementary Figure 5: Estimated marginal response of yields to growing-season rainfall in (mm per month) for maize, rice, and wheat. The straight lines are the gradients of the quadratic response functions estimated using Equation 1 (Methods). Values above the x-axis correspond to a positive response to increased rainfall.



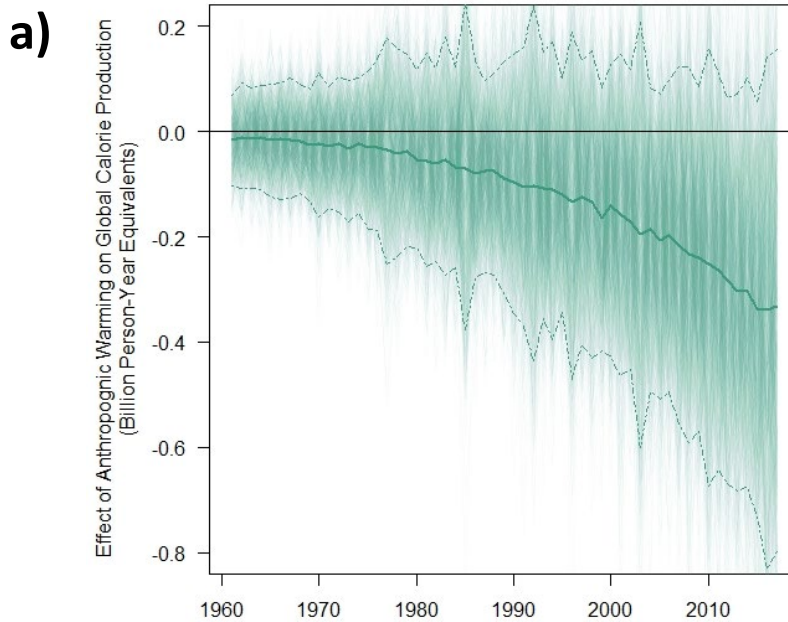
Supplementary Figure 7: Index weightings by crop and country using yield-temperature responses derived from the empirical model (Empirical) and from process-based crop models participating in the AgMIP Phase 2 (AgMIP). A) Maps of index weighting by crop and country for each method. Weighting is based on the estimated signal to noise ratio of the anthropogenic effect of crop yields (Methods). The index is also directional (i.e. takes positive and negative values), accounting for the fact that the same warming signal might have opposite effects on yield depending on the crop and location). B) Comparison of index weights using both temperature response methods. Dotted black line gives the 1:1 line and the solid line is the best-fit linear model through all points, with the shaded area giving the 95% confidence interval.



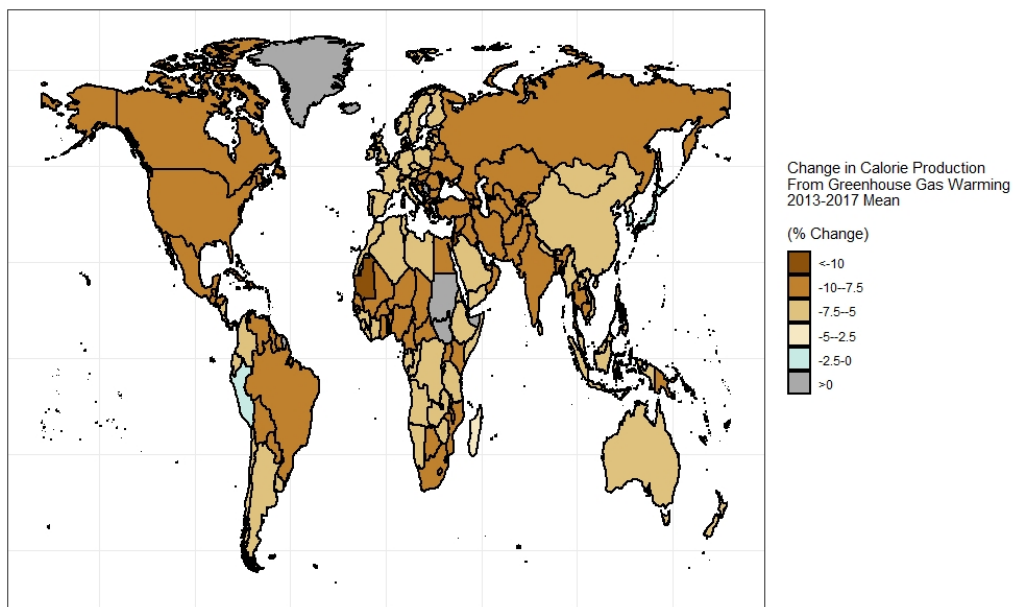
Supplementary Figure 8: As Figure 4a in the main text, but using yield-temperature responses derived from process-based crop models participating in the AgMIP GGCM Phase 2 experiment.



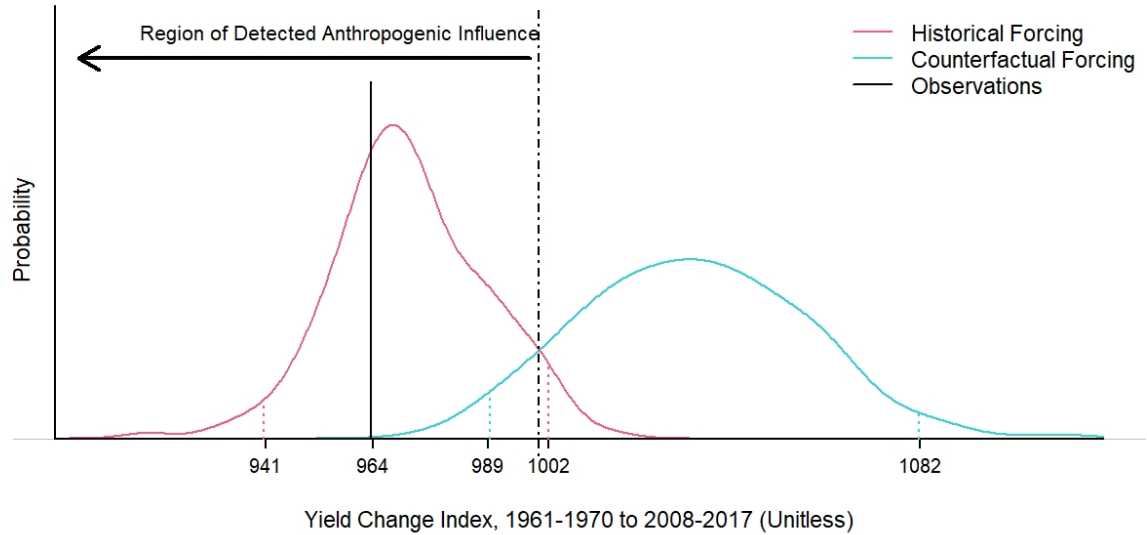
Supplementary Figure 9: Similar to Figure 4a in the main text but showing the distribution of yield change indices under alternate aggregation weightings. a) Aggregation using uniform weights (ie. unweighted). b) Aggregation weighting by average per-capita income over the baseline period (logged) (4). The difference in distribution separation, measured by PNS, between these indices and the optimized index with weights based on the estimated anthropogenic climate signal (shown in Figure 4a) gives an indication of the degree to which the detected signal could be explained either by a uniform slow-down in yield growth (A) or differential yield growth trajectories in developed vs developing countries (B)



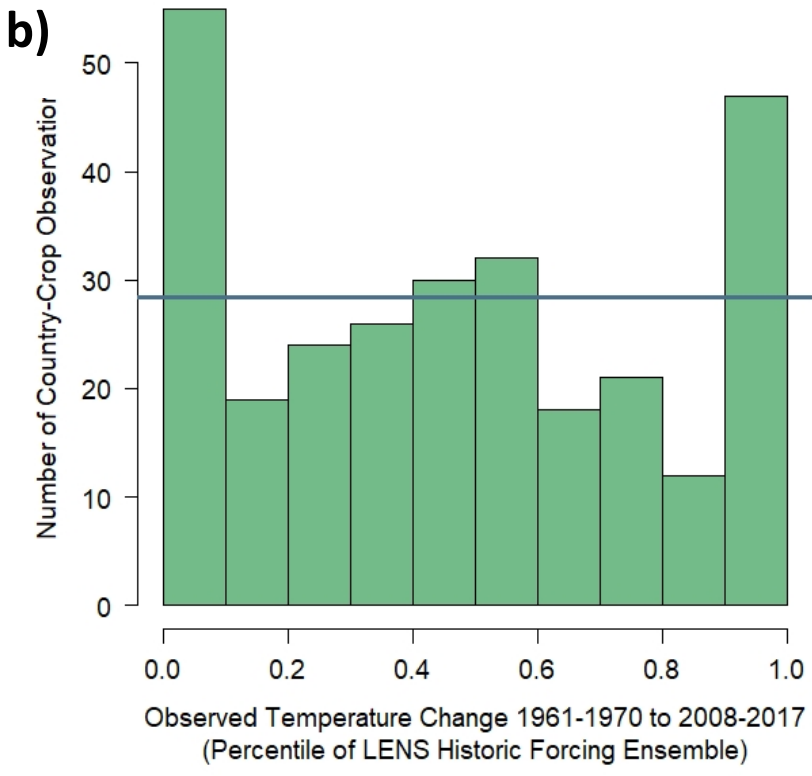
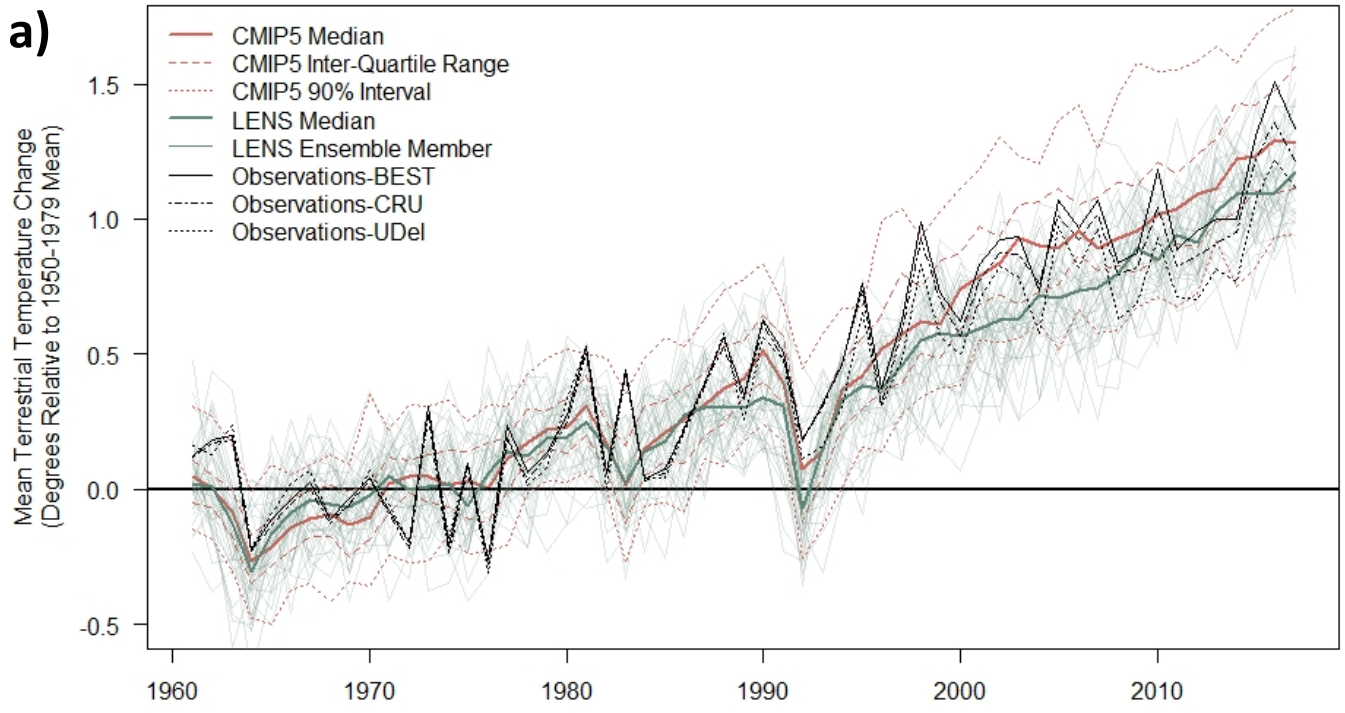
b)



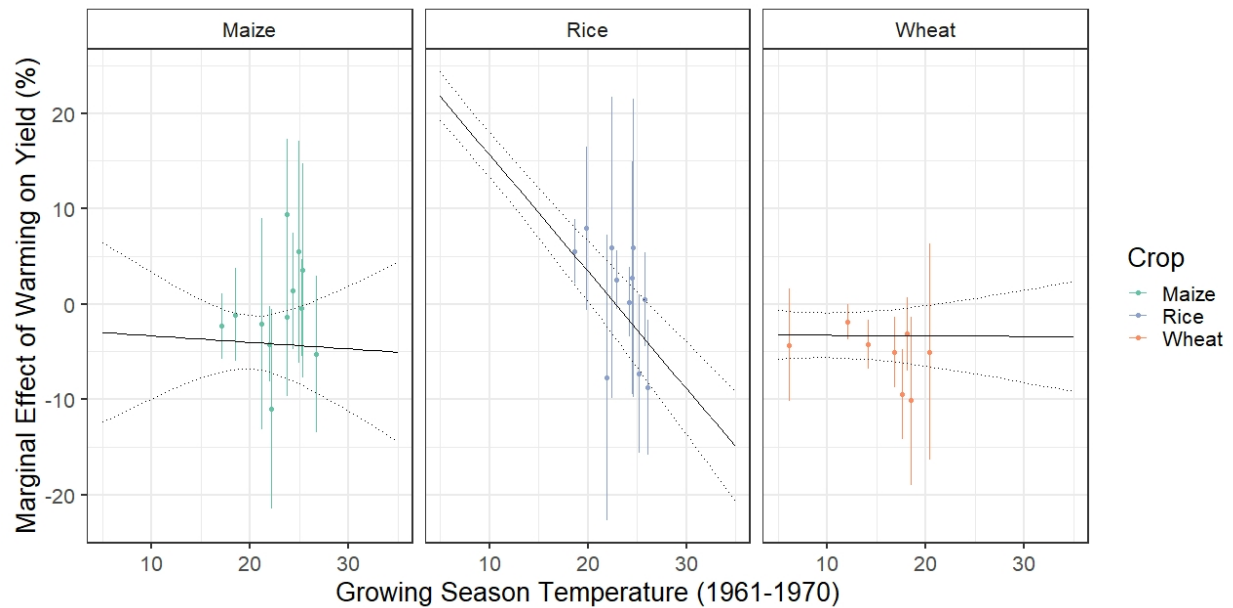
Supplementary Figure 10: Effect of anthropogenic warming on global calorie production. a) Effect of anthropogenic warming on global calorie production from wheat, rice, and maize 1961-2017. Thin lines show 1000 draws from the stochastic simulation used to produce Figure 4, but with aggregation to the global level based on calorie production, rather than the optimized yield index. Solid line shows the mean effect and dashed lines show the empirical 90% confidence interval. Units are in billion person-year equivalents, assuming a caloric requirement of 2,500 calories per day and allowing for 35% post-harvest losses. b) Distribution of caloric change effect by country (2013-2017 mean, % change relative to observed yields).



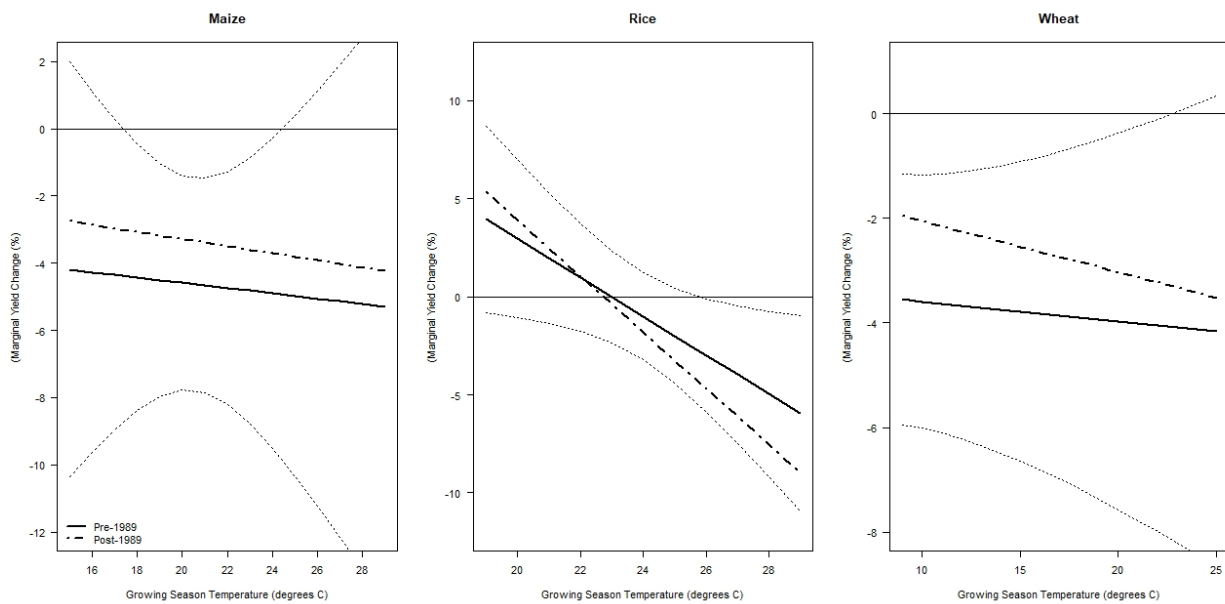
Supplementary Figure 11: Similar to Figure 4a in the main text, but with historical and counterfactual distributions that include internal variability in growing season rainfall. Simulations of the yield index distribution fix growing season rainfall at its observed values. In these simulations, growing season rainfall, like growing season temperature, is sampled from the climate model ensembles. Because there is not a strong signal of anthropogenic emissions on total growing season rainfall (Supplementary Figure 3), this adds variation to both distribution but does not increase the separation, leading to a larger overlap between the historical and counterfactual distributions than seen in Figure 4a. The PNS for these simulations that include internal variability in growing season rainfall drops to 84.9% from 87.3% for the index shown in Figure 4a.



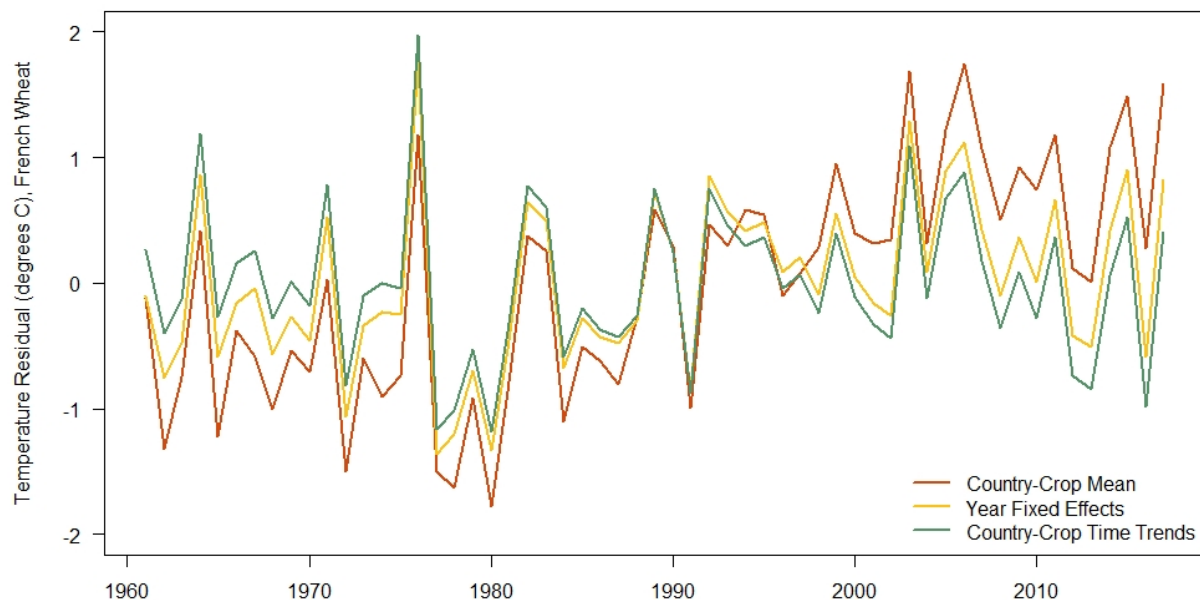
Supplementary Figure 12: Evaluation of temperature changes in the CESM LENS. a) Terrestrial temperature change 1961-2017 relative to the 1950-1979 mean for the LENS historical forcing ensemble (green lines), the CMIP5 ensemble (red lines) and 3 observational datasets (black lines). b) Observed changes in growing season temperature over growing areas for each country-crop combination in the data, as a quantile of the LENS distribution of temperature changes for that crop and country. Horizontal line shows expected value if LENS distribution perfectly matched observed natural variability. Over-representation in the lowest and highest bins implies either noise in observations or an under-estimate of natural variability at this regional scale by CESM.



Supplementary Figure 13: Marginal effects of warming estimated using the full sample (black lines, with 95% confidence interval shown by the dotted lines, same as shown in Figure 2) and estimated in separate panel regressions for each geographic region and crop (requiring at least 5 countries in that geographic region grow that crop). Error bars show the 95% confidence interval for those estimated marginal effects.



Supplementary Figure 14: Marginal effects of warming estimated pre- (solid line) and post-1989 (dashed line). Dotted lines show the 95% confidence interval for the pre-1989 estimate.



Supplementary Figure 15: Figure showing the effect of regression terms on the variation used to estimate the parameters of the yield-temperature response function (Figure 1 b-d), illustrated using the example of French wheat (i.e. temperatures over wheat growing areas in France, during the French wheat growing season). The raw data (red) shows a strong warming trend of 0.03°C per year ($p < 0.001$). Year fixed-effects remove the average global warming effect (yellow line). Since French wheat growing areas are warming slightly faster than the global average, this reduces the warming trend to 0.01°C per year ($p < 0.01$) but does not remove it. The addition of country-crop specific quadratic time trends (green line) fully removes the residual warming trend ($p > 0.5$). This means that the year fixed-effects, country time trends, and temperature response parameters are to some extent co-determined, a fact that will be reflected in the covariance between these estimated parameters and accounted for in the uncertainty sampling scheme used for the detection and attribution analysis.

Supplementary Tables

Dropped Continent	Dropped Crop	PNS	Detection
Asia	Maize	0.880	1
Africa	Maize	0.883	1
Europe	Maize	0.876	1
South America	Maize	0.879	1
Australia	Maize	0.874	1
North America	Maize	0.871	1
Asia	Rice	0.839	1
Africa	Rice	0.862	1
South America	Rice	0.845	1
Australia	Rice	0.872	1
Europe	Rice	0.859	1
North America	Rice	0.868	1
Asia	Wheat	0.873	1
Africa	Wheat	0.872	1
Europe	Wheat	0.871	1
South America	Wheat	0.873	1
Australia	Wheat	0.877	1
North America	Wheat	0.872	1

Supplementary Table 1: Separation of historical and counterfactual index (measured using PNS) and signal detection result after dropping crop-continent combinations from the aggregate yield index. A value of 1 in the “Detection” column indicates the observed index value is within the region consistent with historical forcing.

Dropped Continent	PNS	Detection
Asia	0.850	1
Africa	0.874	1
Europe	0.855	1
South America	0.856	1
Australia	0.873	1
North America	0.864	1

Supplementary Table 2: As Supplementary Table 1, except excluding whole continents, rather than crop-continent combinations from the yield index

Supplementary Methods

De-Transforming Variables for Marginal Effect Plots

The empirical crop model is estimated using temperature and rainfall data normalized by subtracting the historic mean μ and dividing by the standard deviation σ , estimated across the whole dataset. The same normalization (using the same historic μ and σ) is performed on climate model data prior to simulating yield trajectories using the stochastic simulation. Un-normalization is performed only to display the marginal effects of temperature (Figure 2, Supplementary Figures 13 and 14) and rainfall (Supplementary Figure 5) changes, and to compare the marginal effects of warming from the empirical model with results from AgMIP (Supplementary Figure 4). This procedure is described below:

The estimated empirical equation is:

$$y_{itc} = \beta_{1c} \left(\frac{T_{itc} - \mu}{\sigma} \right) + \beta_{2c} \left(\frac{T_{itc} - \mu}{\sigma} \right)^2 = \beta_{1c} \left(\frac{T_{itc} - \mu}{\sigma} \right) + \beta_{2c} \left(\frac{T_{itc}^2 - 2\mu T_{itc} + \mu^2}{\sigma^2} \right)$$

Where y_{itc} is log yield in country i in year t for crop c .

The marginal effect of temperature change is:

$$\frac{dy}{dT} = \frac{\beta_{1c}}{\sigma} + \frac{\beta_{2c}}{\sigma^2} (2T - 2\mu)$$

This gives the marginal effects plotted in Figure 2 for a range of growing season temperatures.

The variance of the marginal effects at temperature T are calculated using the formula for the variance of a linear transformation of a multivariate normal distribution:

$$\text{Var} \left(\frac{dy}{dT} \right) = \mathbf{X}^T \boldsymbol{\Sigma} \mathbf{X}$$

Where \mathbf{X} is a 2 by 1 vector with the first element given by $\frac{1}{\sigma}$ and the second element given by $\frac{2(T-\mu)}{\sigma^2}$ and $\boldsymbol{\Sigma}$ is the 2*2 variance co-variance matrix of the β_{1c} and β_{2c} coefficients. Since maize is the dropped factor in the empirical estimation, calculations for wheat and rice contain two additional terms corresponding to the interactions with the crop indicator. Calculations for rainfall effects shown in Supplementary Figure 5 proceed similarly.

Yield-Temperature Response Derived from AgMIP GGCM Phase 2 Results

As a comparison to the empirical crop model results discussed in the main text, I also use yield-temperature responses derived from an ensemble of process-based crop models participating in the AgMIP Global Gridded Crop Model Intercomparison (GGCM) Phase 2 experiment. This experiment, described in detail in Franke et al. (5), includes up to 12 process-based crop models run on a global grid. Models are systematically perturbed over 5 input variables (CO_2 , Temperature, Rainfall, Applied Nitrogen, and cultivar length). This procedure allows a ceteris-paribus temperature response function, comparable to that estimated from the empirical crop model described in the main text, to be recovered for each participating model. Results in this paper use four models from the GGCM Phase 2 results:

CARAIB (6, 7), EPIC-TAMU (8), LPJ-GUESS (9, 10), and pDSSAT (11, 12). These were the set of models that both provided results for all three crops analyzed in this paper (i.e. rice, maize, and wheat) and were classified as “high participation” in the experiment, meaning the model teams ran a high fraction of the total 756 simulations in the experiment.

Country-crop temperature response functions for each model are estimated by fixing other input dimensions at their experiment-defined “baselines” ($\text{CO}_2 = 360\text{ppm}$, No change in rainfall, 200 kg ha^{-1} applied nitrogen and no change in cultivar length, see 43) and taking area-weighted average yields over each country for each level of temperature change, $\Delta T \in [-1, 0, 1, 2, 3, 4]$. Percent change in yield at each temperature level is defined relative to modeled yield at $\Delta T = 0$. GGCM Phase 2 reports simulations separately for spring and winter wheat. These are combined into an average wheat yield response through a weighted average with weights defined as the area of spring vs winter wheat in 2000 in each country based on area reported in Sacks et al. (13). Marginal effects shown in Supplementary Figure 4 are the % change in yield at $\Delta T = 1$ degree.

Simulating the distribution of alternate yield trajectories under historical and counterfactual forcings, sampling from the uncertainty in the process-based crop yield ensemble, is done as follows:

- 1) Simulate 1000 alternate yield trajectories for all countries and crops for 1961-2017 without temperature change by drawing from the parameter variance-covariance matrix of the empirical model, fixing temperature at the mean in the baseline period (1961-1970) for all country-crop combinations. Calculate the change in yield for each country-crop between the start (1961-1970) and end (2008-2017) period.
- 2) Draw 500 times from the counterfactual climate model ensemble and 500 times from the historical climate model ensemble to simulate alternate temperature trajectories between the start and end period with and without greenhouse gas emissions.
- 3) For each temperature trajectory, draw a sample from the 4 empirical crop models in the GGCM ensemble. Calculate the change in yield for all country-crop combinations under that temperature scenario by linearly interpolating between the GGCM simulation points (i.e. minus 1, 0, 1, 2, 3 and 4 degrees of warming). Yield changes at -1 and 4 degrees warming are assigned for any cooling greater than -1 degrees or warming greater than 4 degrees respectively.
- 4) Apply estimated yield changes to the end period yields simulated in step 1

For each simulation, country-crop yield changes between the start and end periods are aggregated into a yield index using a weighting scheme derived using the procedure described in the main text. Weights for the AgMIP-based index and a comparison with weights using the temperature response from the empirical crop model are given in Supplementary Figure 7.

1. C. Monfreda, N. Ramankutty, J. A. Foley, Farming the planet: 2. Geographic distribution of crop areas, yields, physiological types, and net primary production in the year 2000. *Global Biogeochem. Cycles* **22**, n/a-n/a (2008).
2. I. Harris, T. J. Osborn, P. Jones, D. Lister, Version 4 of the CRU TS Monthly High-Resolution Gridded Multivariate Climate Dataset. *Sci. Data* **7**, 109 (2020).
3. A. Hannart, *et al.*, Causal Counterfactual Theory for the Attribution of Weather and Climate-Related Events. *Bull. Am. Meteorol. Soc.* **97**, 99–110 (2016).
4. R. C. Feenstra, R. Inklaar, M. P. Timmer, The Next Generation of the Penn World Table. *Am. Econ. Rev.* **105**, 3150–3182 (2015).
5. J. Franke, *et al.*, The GGCM Phase II experiment: global gridded crop model simulations under uniform changes in CO₂, temperature, water, and nitrogen levels (protocol version 1.0). *Geosci. Model Dev. Discuss.*, 1–30 (2019).
6. M. Dury, *et al.*, Responses of European forest ecosystems to 21st century climate: assessing changes in inter-annual variability and fire intensity. *iForest Biogeosciences For.* **4** (2011).
7. N. Pirttioja, *et al.*, Temperature and precipitation effects on wheat yield across a European transect: A crop model ensemble analysis using impact response surfaces. *Clim. Res.* **65**, 87–105 (2015).
8. R. C. Izaurralde, J. R. Williams, W. B. McGill, N. J. Rosenberg, M. C. Q. Jakas, Simulating soil C dynamics with EPIC: Model description and testing against long-term data. *Ecol. Modell.* **192**, 362–384 (2006).
9. M. Lindeskog, *et al.*, Implications of accounting for land use in simulations of ecosystem carbon cycling in Africa. *Earth Syst. Dyn.* **4**, 385–407 (2013).
10. S. Olin, *et al.*, Modelling the response of yields and tissue C : N to changes in atmospheric CO₂ and N management in the main wheat regions of western Europe. *Biogeosciences* **12**, 2489–2515 (2015).
11. J. Elliott, *et al.*, The parallel system for integrating impact models and sectors (pSIMS). *Environ. Model. Softw.* **62**, 509–516 (2014).
12. J. W. Jones, *et al.*, The DSSAT cropping system model. *Eur. J. Agron.* **18**, 235–265 (2003).
13. W. J. Sacks, D. Deryng, J. A. Foley, N. Ramankutty, Crop Planting Dates: An Analysis of Global Patterns. *Glob. Ecol. Biogeogr.* **19**, 607–620 (2010).